

Epitaxial Cobalt Oxide Films with Wurtzite Structure on Au(111)

Maximilian Ammon, Sara Baumann, Tilman Kießlinger, Janek Rieger, Thomas Fauster, Josef Redinger, Lutz Hammer,* and M. Alexander Schneider*

Several-nanometer-thick, closed, and epitaxial cobalt(II) oxide films with wurtzite crystal structure (w-CoO) are grown on Au(111) and their structural and electronic properties analyzed. The structural quality of the (000 $\bar{1}$) oriented, oxygen-terminated, and unreconstructed films allow the application of surface-science methods to unravel the properties of this unusual polymorph of CoO and may pave the way for future thin-film applications. An experimental structural analysis by low-energy electron diffraction (LEED-IV) is presented with an excellent agreement between measured and calculated intensity spectra expressed by a Pendry R-factor of $R = 0.112$ and few-picometer error bounds in the parameter values. Using scanning tunneling spectroscopy (STS) the bandgap of the semiconducting films is found to be 1.4 ± 0.2 eV. Ultraviolet photoelectron spectroscopy (UPS) confirms the presence of a gap and the position of the Fermi level (E_F). The structural results of density functional theory calculations using (hybrid) functionals to treat electron correlations and van der Waals forces agree well with the experimentally determined structure of the antiferromagnetic w-CoO films. In contrast to generalized gradient approximation (GGA)+U calculations, the Heyd–Scuseria–Ernzerhof hybrid functional reproduces the semiconducting nature correctly and predicts surface states in the gap which might pin E_F in agreement with STS and UPS.

1. Introduction

Polymorphism in materials is not only of fundamental scientific interest but it also offers new fields of application in sensing, energy and data storage, catalysis, optical devices, etc., which are important for future technological development. A major obstacle is the reliable fabrication of metastable polymorphs for which the conversion into the thermodynamically stable phase requires an external trigger. The wurtzite polymorph of cobalt oxide (in the following: w-CoO, space group $p6_3mc$) was prepared and detected (among other CoO phases) in 1962 by Redman and Steward in nanocrystalline powders produced from cobalt acetate.^[1] It took 40 years until Risbud et al. could prepare a pure w-CoO powder.^[2] In their recent review, Nam et al. summarized preparation methods to obtain nanosized crystalline w-CoO by tuning reaction kinetics.^[3]

The metastable w-CoO allows reaction pathways for the preparation of, e.g., electrochemical or sensing electrodes that are not accessible via the stable compounds rocksalt (rs-) CoO or spinel Co_3O_4 .^[4–6] A machine-learning analysis of the potential energy surface of the cobalt oxide phases was recently realized by Kong et al.^[7] The ongoing and recent interest in CoO is due to its role in electro- and photocatalysis and due to its antiferromagnetic (AFM) properties. In the field of solar power technology and hydrogen-related catalysis, Wang et al. showed that w-CoO exhibits a direct bandgap suitable as a photovoltaic absorber.^[8] Other studies highlighted the superior catalytic properties of w-CoO nanocrystallites^[9] and w-CoO-type 2D islands.^[10]


For experimental investigations of the potential of w-CoO an ideally single-crystalline alternative to the chemically prepared nanocrystalline material is highly desirable. This would allow to identify reaction mechanisms, e.g., the role of defects or edges in catalysis^[9,10] or to clarify the magnetic order in w-CoO and its Néel temperature which might depend on particle size and interface properties.^[11,12] Today there is a broad consensus, that w-CoO is an antiferromagnet, but unraveling the details is an ongoing challenge for experiment and theory.^[11,13–17]

So far, w-CoO films were prepared by pulsed laser deposition on a ZnO buffer layer on a sapphire substrate^[14] or from Co-doped ZnO films as nanocrystalline, embedded phase.^[18] Only recently micrometer-thick polycrystalline w-CoO films were

M. Ammon, S. Baumann,^[†] T. Kießlinger, J. Rieger, T. Fauster, L. Hammer, M. A. Schneider

Lehrstuhl für Festkörperphysik
Friedrich-Alexander Universität Erlangen-Nürnberg
Staudtstrasse 7, 91058 Erlangen, Germany
E-mail: lutz.hammer@fau.de; alexander.schneider@fau.de

J. Redinger
Institut für Angewandte Physik and Center for Computational Materials Science
Technische Universität Wien
Wiedner Hauptstrasse 8-10/134, 1040 Vienna, Austria

 The ORCID identification number(s) for the author(s) of this article can be found under <https://doi.org/10.1002/pssr.202100383>.

^[†]Present address: Institute for Solar Energy Research Hamelin (ISFH), Am Ohrberg 1, 31860 Emmerthal, Germany

© 2021 The Authors. physica status solidi (RRL) Rapid Research Letters published by Wiley-VCH GmbH. This is an open access article under the terms of the Creative Commons Attribution License, which permits use, distribution and reproduction in any medium, provided the original work is properly cited.

DOI: 10.1002/pssr.202100383

produced on a glass substrate by DC magnetron sputtering.^[8] While the latter may be applicable in device production, these methods lack the epitaxial orientation of films and the well-defined surfaces produced by deposition and oxidation of cobalt in ultrahigh vacuum (UHV) that can be obtained for other polymorphs, e.g., on Ir(100),^[19–22] on Pd(100),^[23] and on Ag(100).^[24,25] Films that could be called epitaxial w-CoO films have so far only been produced in the one or two CoO bilayer (BL) regime.^[26–31] However, up to that thickness these films cannot be distinguished from rs-CoO(111) films with wurtzite surface termination.^[32] With our work, we provide a method to grow several-nanometer-thick w-CoO films epitaxially on Au(111). Furthermore, we analyze the structural and electronic properties of the pristine w-CoO(000 $\bar{1}$) surface.

2. Results

2.1. Growth and Thermal Stability of w-CoO Films

We have investigated the growth of cobalt oxide films on a Au(111) substrate for various temperatures, film thicknesses and oxygen pressures. It turns out that at fixed Co flux the emergence of w-CoO depends sensitively on the oxygen partial pressure p_{ox} in agreement with the study by Wang et al.^[8] The results presented here were obtained at a fixed Co flux of $\approx 2 \times 10^{13}$ atoms $\text{s}^{-1} \text{cm}^{-2}$ and for $p_{\text{ox}} \approx 5 \times 10^{-7}$ mbar, where w-CoO was found to develop best. Wurtzite CoO films were also obtained by other combinations of Co flux and p_{ox} but this was not investigated in detail.

Our investigation covers a wide range of film thicknesses from sub-monolayer coverage ($\Theta \approx 0.4$ BL) via ultrathin films ($\Theta \approx 3$ –4 BL) up to “bulk-like” 4 nm thick films ($\Theta \approx 15$ BL).

Upon annealing to 200–350 °C in UHV, the structural order improved and all investigated w-CoO films showed a sixfold symmetric hexagonal low-energy electron diffraction (LEED) pattern (Figure 1). For lower thicknesses (0.4 and 4 BL), it is overlaid not only by the diffraction spots of the Au(111) substrate, but also by satellite spots (see insets of Figure 1a,c) indicating a moiré-like superposition of both lattices. In contrast, for the 15 BL film both substrate and moiré spots are absent. This proves that the film is closed everywhere and thick enough such that the interface to the substrate cannot be probed anymore due to the short mean free path of the electrons at the used energies. We evaluate the lateral lattice parameter a_p of the grown films from the mutual distance of the diffraction spots (with the Au(111) spots taken as a reference) resulting in values of $a_p = 3.14$ – 3.26 Å depending on film thickness.

These lattice parameters rule out the presence of rocksalt CoO (rs-CoO, $a_p = 3.01$ Å) or spinel-type Co_3O_4 ($a_p = 5.72$ Å) within the film, but suggest a wurtzite or zincblende crystal structure, for which a_p values between 3.21 and 3.24 Å are reported.^[1,2,8] By LEED-IV (see Section 2.1.1), we prove that the films are oxygen-terminated w-CoO in (000 $\bar{1}$) orientation.

Our findings for low coverage are in agreement with previous work.^[27,28] Wurtzite CoO starts to grow in islands on Au(111) that coalesce to form an almost closed film (Figure 1a,b). In scanning tunneling microscopy (STM), the film has an apparent height of 4–5 Å depending on bias voltage in good agreement with the geometrical thickness of a double bilayer (DBL) film. A pronounced

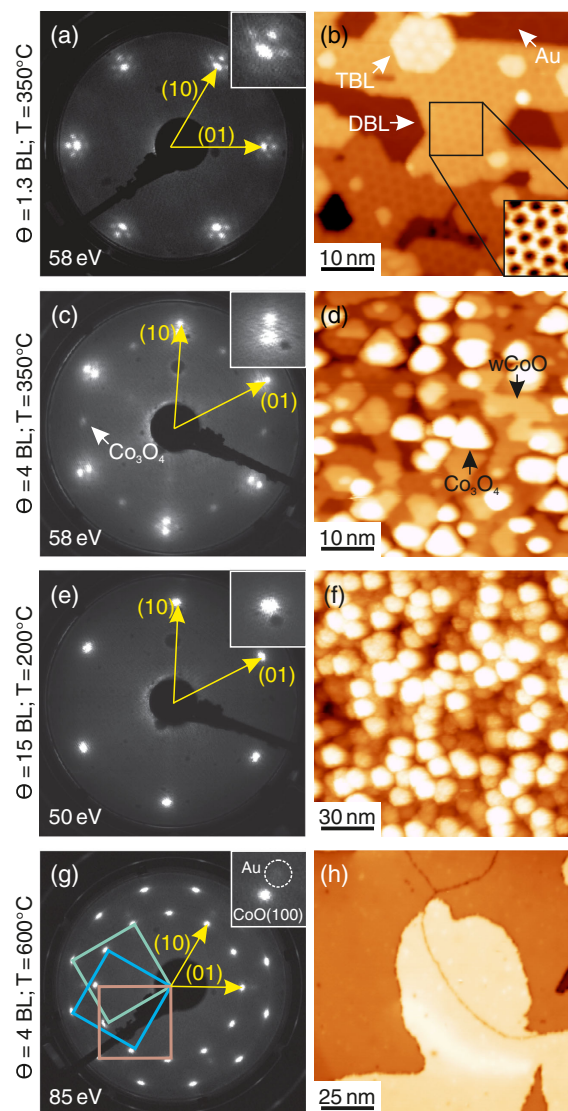


Figure 1. LEED pattern (left) and STM images (right) of CoO films of different coverages and annealing temperatures. a,b) Sub-monolayer coverage ($\Theta \approx 0.4$ BL), c,d) few monolayer coverage ($\Theta \approx 4$ BL), e,f) a thick film with $\Theta \approx 15$ BL thickness. g,h) Same film as in (e,f), but further annealed to 600 °C. Three rotational domains of rs-CoO(100) are identified. The insets of the LEED images magnify the region around the (1 0) beam. Note the different alignment of the crystal in (g). STM parameters: b) +5.0 V, 100 pA; d) +5.0 V, 75 pA; f) +5.0 V, 100 pA; h) +3.0 V, 200 pA.

moiré pattern with a period $a_m = 29.0 \pm 0.2$ Å is observed in STM as well as in LEED (see insets of Figure 1a,b) and indicates local distortions at the interface to the substrate. This moiré pattern continues to triple BL (TBL) coverage. Corresponding islands in Figure 1b show a characteristic contrast inversion of the moiré pattern in STM with respect to that of the DBL film, in agreement with observations made by Fester et al. (called multilayer there).^[28]

With increasing CoO deposition, the remaining bare substrate patches vanish. Terrace steps have heights of about 2.5 Å, corresponding to a single BL spacing (Figure 1d). Starting from $\Theta \approx 4$ BL, we additionally observe the growth of a competing,

ordered phase leading to extra diffraction spots in LEED (one is marked by an arrow in Figure 1c). We interpret the small, triangular grains visible in Figure 1d (one is marked by an arrow) to belong to this extra phase. The minority phase is identified as $\text{Co}_3\text{O}_4(111)$ by comparing the LEED-IV spectra of the extra spots with those from extended, spinel-type $\text{Co}_3\text{O}_4(111)$ films grown on $\text{Ir}(100)$.^[20] The coexistence of Co_3O_4 and w-CoO was also observed when oxidizing nanosized w-CoO in air but attributed to a transition via rs-CoO.^[3]

The growth of this $\text{Co}_3\text{O}_4(111)$ phase can be suppressed by reducing the post-annealing temperature to 200 °C. In this way it is possible to grow a monophase, epitaxial w-CoO film on $\text{Au}(111)$ proven by LEED, where the aforementioned extra spots have completely vanished (Figure 1e). Due to the lower annealing temperature the long-range order has deteriorated somewhat (cf. Figure 1f), with average grain diameter of 11 ± 2 nm and a surface roughness of 5 ± 1 Å.

The w-CoO films are metastable and convert into rs-CoO upon annealing to above 350 °C in UHV. If a perfect w-CoO preparation was achieved (i.e., with no spinel Co_3O_4) the films convert to rs-CoO(100) (Figure 1g,h), otherwise CoO(111) films are produced.

2.1.1. Crystallographic Structure

To prove the wurtzite-type film structure, we carried out a LEED intensity analysis for the 15 BL thick CoO-film (Figure 1e). Due to the sixfold degeneracy of the LEED beams, averaging over symmetry-equivalent beams led to five independent $I(E)$ -spectra only. These were taken in the energy range 45–600 eV resulting in a total data basis of $\Delta E = 2118$ eV, more than sufficient to adjust six structural and five nonstructural parameters in the course of the analysis (redundancy factor $\rho = 8.8$).

In a first rough analysis, we tested different structural models. Guided by the lateral lattice parameter of $a_p = 3.26$ Å derived from the LEED pattern, we restricted this comparison to wurtzite and zincblende structures only, both with either Co or O surface termination. This model survey clearly favored the wurtzite-type stacked and oxygen terminated model with a Pendry R-factor of $R = 0.20$, whereas all other models led to R-factor values of $R = 0.41$ – 0.61 and could therefore be discarded with confidence. Also, attempts to introduce stacking faults into the wurtzite structure or to compensate the (formal) polarity by an OH-termination always led to an increase of the R-factor level. Hence, by virtue of this low R-factor and the (1×1) unit cell (Figure 1e), we can exclude an OH-termination or a surface reconstruction experimentally with confidence. The $(000\bar{1})$ oxygen surface termination is inverse to that of the w-CoO nanocrystals embedded in a $\text{ZnO}(0001)$ matrix prepared by Meyerheim et al.^[18] It appears that in that case the external ZnO matrix overrides the natural growth direction of w-CoO.

In the subsequent refinement of the fit, we independently varied the outermost three layer distances as well as the vibrational amplitudes of top O and Co atoms on a very fine grid (steps of 0.0025 and 0.005 Å, respectively). We also considered that no precise values for w-CoO bulk lattice parameters (a_p , $c/2$, and $d_{\text{O-Co}}$, cf. Figure 2) are available. Therefore, we additionally had to adjust these parameters in our fit, while bulk vibrational amplitudes were taken identical to those for rs-CoO with Debye

temperature $\Theta_D = 518$ K.^[33] For computational and fitting details see the Supporting Information. Eventually, a bestfit structure was found characterized by an R-factor of $R = 0.112$. The excellent quality of the fit is visualized by a comparison of all measured and calculated spectra shown in Figure 2a.

A compilation of all structural parameter values (including error margins) determined by our LEED analysis is shown in Table 1, nonstructural parameters in Table S1, Supporting Information.

2.1.2. Electronic Properties

We studied the electronic properties of w-CoO by scanning tunneling spectroscopy (STS) and ultraviolet photoemission spectroscopy (UPS). As shown in Figure 3a, averaged STS conductance curves $G(V) = dI/dV(V)$ where V is the tunneling bias voltage were recorded for different w-CoO thicknesses: on DBL islands, on a nominally 3 BL thick closed film, and a bulk-like film ($\Theta \approx 15$ BL). Spectra from TBL or 4 BL high grains present in the 3 BL film are indistinguishable in experiment and therefore both are included in the average. The spectra taken on nominally 3 and 15 BL thick films display a clear semiconducting behavior with a bandgap increasing with thickness. In contrast, on DBL islands a finite conductivity at $V = 0$ V bias is observed. This could point to a metallic character of the DBL film. However, the spectrum exhibits a ≈ 300 mV wide region of low conductivity around zero bias that could be interpreted as a gap feature. In this case, the finite conductivity would be caused by electron tunneling through the ultrathin film in the bandgap energy region.

The procedure applied to extract the band onsets, the valence band maximum (VBM) E_V and the conduction band minimum (CBM) E_C is described in the Supporting Information. For the 15 BL films, we find a bandgap of $E_g = 1.4 \pm 0.2$ eV which is slightly smaller than that found in optical experiments.^[8] Averaging STS data taken on 3 BL and 4 BL thick w-CoO (nominally 3 BL thick film) results in $E_g = 0.6 \pm 0.2$ eV.

To exclude effects of the electric field in the tunneling junction on E_g , we carried out UPS on a nominally 13 BL thick film. The resulting spectrum is shown in Figure 3b. No photoemission intensity could be detected several 100 meV below E_F supporting the semiconducting nature of the film. By linear extrapolation of the VBM edge in the UPS spectrum, we find the onset energy of the valence band to be $E_V - E_F = -0.7 \pm 0.1$ eV which compares well to the value of $E_V - E_F = -0.6^{+0.05}_{-0.25}$ eV obtained by STS. This points to only little influence of the electric field in the STM as tip-induced band bending would lead to a lower measured E_V .^[34] Furthermore, by UPS, we determined the work function of the w-CoO(000 $\bar{1}$) film to be 4.6 ± 0.1 eV which is significantly lower than that of rs-CoO(100) (5.17 eV) or rs-CoO(111) (5.91 eV).^[35]

3. Discussion

We compare our experimental findings to literature and our density functional theory (DFT) calculations. The detailed DFT results are given in Figure S2, S3, and Table S2, Supporting Information. It is well known that electron correlation in the

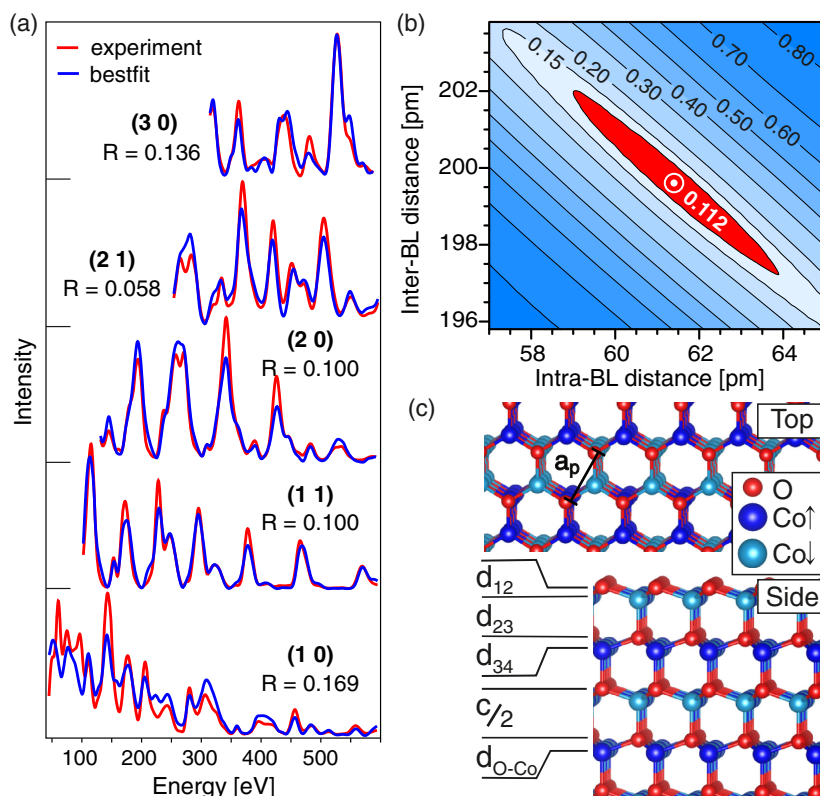


Figure 2. a) Compilation of experimental and corresponding bestfit LEED-I(E) spectra. b) R-factor plot visualizing the correlation of intra- and inter-BL distances. The area marked in red corresponds to the range of error, where the R-factor is below the variance level of the analysis. c) Ball model of the wurtzite structure with definition of the vertical parameters varied in the LEED analysis. The colors of the Co atoms indicate the AF1 antiferromagnetic order used in the calculations. For labeling, the different AFM configurations see the study by Han et al.^[15]

Table 1. Compilation of fitted structural parameters and error margins from the LEED-IV analysis. The absolute parameter values obtained from the PBE + U + TS ($U_{\text{eff}} = 4$ eV) and HSE06 slab calculations ($\alpha = 0.25$) in AF1 configuration are given for comparison. All values are given in Å. For symbols, see Figure 2.

Parameter	LEED		PBE + U + TS	HSE06
a_p	3.263	+0.020 -0.025	3.238	3.259
$c/2$	2.610	+0.007 -0.008	2.590	2.614
d_{O-Co}	0.612	+0.031 -0.033	0.615	0.612
d_{12}	0.405	+0.089 -0.083	0.368	0.367
d_{23}	1.995	+0.021 -0.014	1.972	1.999
d_{34}	0.593	+0.024 -0.015	0.605	0.593

3d transition metal oxides call for DFT treatments beyond LDA or generalized gradient approximation (GGA). There are ample examples in literature where different approximations are compared among each other and with experiments of which most concentrate on rs-CoO^[36–40] and only few on w-CoO.^[13,15,41] There have been attempts to determine the value of the Hubbard U from physical properties rather than as a fitting parameter,^[37] and the suggested value adopted by most authors

is $U_{\text{eff}} = 4$ eV for rs-CoO with the exception of Han et al. and Wang et al., who use $U_{\text{eff}} = 6$ eV.^[8,13,15] Even the precise structure determination presented here does not constrain the choice of U_{eff} (Figure S3, Supporting Information).

While adding a Hubbard U term to GGA exchange functionals reproduces the semiconducting nature of bulk CoO, it fails to predict the correct energetic hierarchy of the CoO polymorphs. Our PBE + U and Heyd–Scuseria–Ernzerhof (HSE) calculations predict that bulk w-CoO is energetically more favorable than rs-CoO independent of appropriate parameter ranges $2 \text{ eV} < U_{\text{eff}} < 6 \text{ eV}$ or $0 < \alpha < 0.4$. Only for $\alpha > 0.4$ do the HSE calculations predict the rocksalt structure to be the most stable and zincblende the least stable polymorph of CoO. In line with the findings of Peng and Perdew,^[42] adding vdW interactions lifts this inadequacy and results in rs-CoO to be the most stable polymorph for choices of $U_{\text{eff}} > 2.0$ eV for the Tkatchenko–Scheffler (TS) and for $U_{\text{eff}} > 3.5$ eV for the Grimme D3 method (see Section 5 and Figure S2, Supporting Information). For the used functionals, these results agree with those obtained by Saritas et al.^[41] However, we find that the zincblende and wurtzite polymorphs never differ by more than 23 meV per formula unit which we attribute to the slightly different AFM configurations used for the zincblende polymorph in both studies. The dependence of the total energy of the polymorphs on the chosen functional questions the conclusions of the potential energy

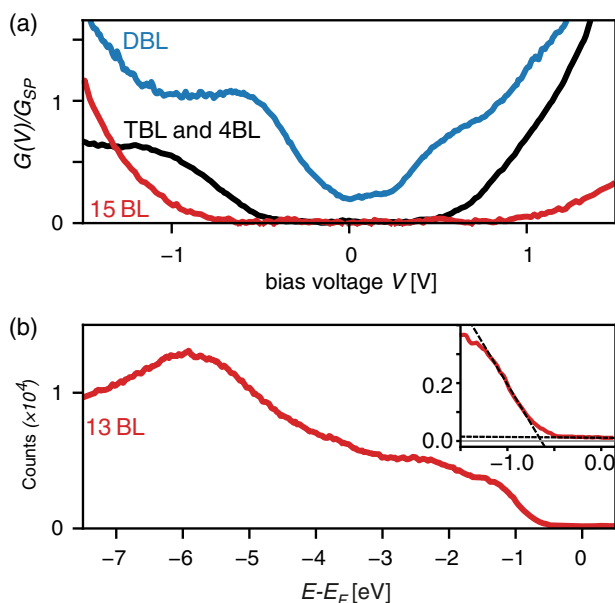


Figure 3. a) Normalized and averaged conductivity $G(V) = dI/dV(V)$ versus bias voltage U taken for w-CoO films of different thicknesses. G_{SP} denotes the conductivity of the tunneling junction prior to opening the feedback loop. The spectrum taken on a DBL film has finite conductivity at zero bias voltage. b) UPS data for a 13 BL w-CoO film. The data show a gap at the Fermi energy E_F . By linear extrapolation (insert, dashed lines), the VBM is determined.

surface analysis provided by Kong et al.^[7] who, in view of the lower total energy of w-CoO in the absence of vdW corrections, emphasized the importance of defects for the experimentally observed “uphill” w-CoO to rs-CoO transition.

In the following, we quote the results of the slab calculations using PBE + U + TS with $U_{\text{eff}} = 4$ eV and HSE06 ($\alpha = 0.25$) as these fall with their prediction of the absolute values of the bulk parameters $d_{\text{O-Co}}$, a_p , and $c/2$ within the error bounds of the LEED analysis (Table 1). However, when scaling a_p to the experimental value, the error bounds of the LEED analysis do not allow to discard any of the tested functionals on structural reasons.

Concerning the AFM order, our calculations confirm the expectation that the structural influence is small (Figure S3, Supporting Information). In the following, we consider properties of the AF1 configuration only (shown in Figure 2c). This configuration was calculated to be energetically almost degenerate with the lowest energy collinear state AF3 but ≈ 40 meV more favorable than ferromagnetic Co planes stacked antiferromagnetically along the c -axis (AF2b configuration).^[15] Hence, AF1 serves as a good approximation to the true ground state at lower computational cost.

Scrutinizing the bulk parameters of Table 1, we find that the “bulk” parameters $c/2 = 2.61 \pm 0.01$ Å (half the vertical lattice parameter c) and $a_p = 3.26 \pm 0.02$ Å are in very good agreement with our DFT results and with values derived by X-ray and neutron diffraction for nanocrystalline w-CoO (2.602 and 3.244 Å, respectively).^[2] The experimentally determined intra-BL distance $d_{\text{O-Co}} = 0.61 \pm 0.03$ Å also agrees with the DFT results. In fact, the experimental $d_{\text{O-Co}}$ with its error bound is

largely incompatible with calculations using the AF2b order (Figure S3, Supporting Information). Our experimental and theoretical findings are at variance with $d_{\text{O-Co}} = 0.438$ Å determined from the data given by Risbud et al.^[2] According to our analysis, the films have quite equal axial and “equatorial” Co–O bond lengths of 2.00 Å and 1.98 Å (DFT: the same values for HSE06, 1.98 Å both for PBE + U + TS), while Risbud et al. arrive at remarkably different values of 2.164 ± 0.001 Å and 1.923 ± 0.003 Å—a rather unusual finding as the authors state.

Apart from the possibility that there might be an intrinsic structural difference between Au-supported films and nanocrystalline w-CoO, we also critically checked our analysis for potential artifacts. Especially, for the inter- and intra-BL distances, we found a strong parameter coupling in our fit, leaving their sum $c/2$ to remain constant reliably. This parameter coupling is visualized by the strongly elongated ellipse of the error range within the R-factor shown in Figure 2b. Moving along the diagonal line of constant $c/2$ just describes a vertical shift of the much weaker scatterer O within a rigid lattice made up by the stronger scattering Co ions. In our analysis, this leads to error margins of about 0.03 Å for the axial and 0.01 Å for the “equatorial” Co–O bond lengths, by far too small to account for the discrepancies to the analysis by Risbud et al.^[2] We cannot judge here, whether similar parameter couplings also take place in the X-ray and neutron diffraction analyses cited earlier, to account for the otherwise hardly explicable structural discrepancies between both analyses. We also want to mention that Meyerheim et al. found in their embedded w-CoO nanocrystals axial Co–O bond lengths in the range of 1.87–1.98 Å thus being even slightly smaller than our value of 2.00 Å. However, these values might be strongly affected by the surrounding ZnO matrix and therefore be unsuitable for extended w-CoO crystals.

The only noticeable surface-induced relaxation revealed by our LEED analysis is a 0.21 Å contraction found for the topmost oxygen layer ($d_{12} = 0.41$ Å), also in close agreement with the DFT prediction, while all layer distances below turn out bulk-like within the error margins. Such a strong inward relaxation may be expected for polar ionic surfaces because of the unbalanced electrostatic forces. However, this remarkably strong contraction leads to a shortening of the corresponding outermost Co–O bond length by only 0.05 Å, very similar to what has been observed for the wurtzite-terminated rs-CoO(111) surface.^[32]

The presence of the surface with its relaxation has consequences for the electronic properties of the films. As shown in Figure 4, the layer-resolved density of states within the framework of all used functionals reveal significant changes in the density of states (DOS) of the surface layer but not of the layers below. Consistent with the layer-resolved DOS, a Bader analysis^[43–45] finds the surface CoO BL positively charged with 0.24e (PBE) or 0.27e (HSE) per CoO unit where $-e$ is the charge of an electron. PBE puts more of the charge on the O ion ($-1.07e$ vs $-1.21e$ in the bulk), whereas in HSE the Co ion contributes more ($+1.43e$ vs $+1.27e$ in the bulk).

All functionals predict states arising in the bulk energy gap and significantly enhanced DOS of the CBM region (beyond $E - E_F > 1$ eV) which has only very low DOS for bulk w-CoO.^[8] Significantly, the PBE + U(+TS) calculations for $2 \text{ eV} \leq U_{\text{eff}} \leq 6 \text{ eV}$ predict a metallic surface at variance with

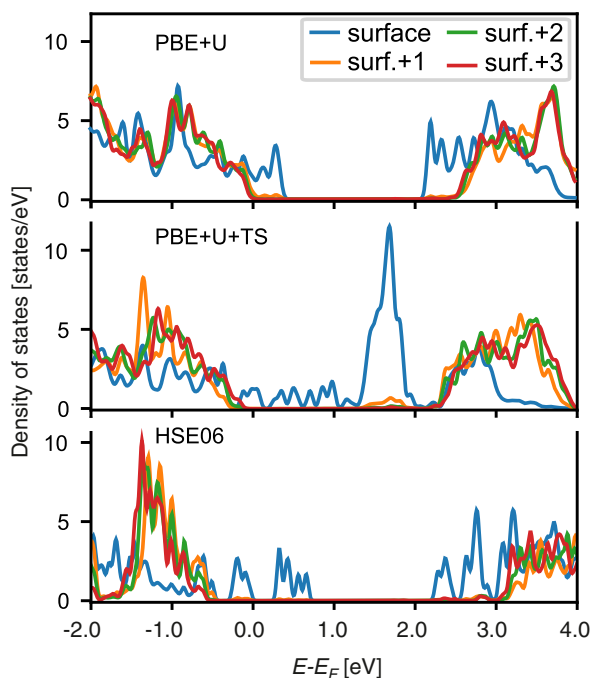


Figure 4. (Bi-)Layer resolved density of states of a 8 BL w-CoO slab for three different functionals. For the PBE + U and PBE + U + TS calculations $U_{\text{eff}} = 4$ eV and for HSE06 $\alpha = 0.25$ was chosen. E_F is the energy of the highest occupied state of the DFT calculations.

the experimental findings. In contrast, the HSE06 calculations arrive at surface-layer states in the energy gap that are clearly split off from the valence band region. These states determine the position of the highest occupied electronic level of the calculation. Its position relative to the bulk VBM is quite consistent with E_F of the STS and UPS experiments. The surface states are, however, not confirmed by spectroscopy. A possible reason could be that in an STS experiment such gap states are often not accessible because of the inhibited electron transport to the bulk contact or too low DOS^[46,47] Similarly, the sensitivity of our UPS setup might not be sufficient to detect these gap states.^[48]

4. Conclusion

With our study, we present a route to grow homogeneous wurtzite-type CoO films of variable thickness which are closed and—most importantly—epitaxially aligned on a Au(111) single-crystal substrate. For the successful growth of such films, it is pivotal to establish the correct oxygen partial pressure during the deposition of metallic Co and carefully adjust postdeposition thermal treatments while controlling the crystallographic structure. This result enables the application of the whole wealth of surface-science techniques to study the physical and chemical properties of this metastable CoO polymorph on a rather easy to handle and versatile support.

By a structural LEED-IV analysis, we determined the crystallographic structure of the w-CoO films with accuracy in the single-digit picometer range. The excellent fit quality is evident from a Pendry R-factor of $R = 0.112$. We find that the

films are oriented with their oxygen-face towards vacuum ($(000\bar{1})$ -termination) at variance to previous reports on w-CoO grains embedded in a ZnO matrix. Furthermore, our analysis further reveals a strong inward relaxation of the outermost oxygen layer.

STS and UPS measurements show that the films are semiconducting. The bandgap of wurtzite CoO is 1.4 ± 0.2 eV when measured by STS and from UPS its work function is determined to be 4.6 ± 0.1 eV. The structural analysis is supported by DFT calculations when electron correlation interaction is accounted for (PBE + U or HSE06). The agreement of the PBE + U calculation improves when vdW interactions are considered (PBE + U + TS). The calculations reveal significant changes in the layer-resolved density of states in the surface layer only. While PBE + U calculations incorrectly predict the surface layer to be metallic, HSE06 points to a Fermi-level pinning by gap states which is compatible with the experimental results from STS and UPS. The gap states at the surface may be significant for the chemical properties of wurtzite cobalt oxide and also for its application as photovoltaic material.

5. Methods Section

Experimental: Our LEED, STM, and UPS experiments were carried out in three independent UHV systems (operating pressure $p \approx 2 \times 10^{-10}$ mbar) all equipped with home-built three-grid LEED optics (ErLEED 150, Specs GmbH) allowing to control and verify the respective film preparations. LEED intensity versus energy (IV) spectra for structural analysis were taken at 100 K, STM images and tunneling spectra at 80 K sample temperature. The photoelectron spectra were recorded at 80 K using a commercial He(I) discharge lamp and a hemispherical analyzer. The He-satellite lines were subtracted. Further details are given in the Supporting Information.

For all experiments we used the same Au(111) single crystal that was cleaned by repeated cycles of 1.5 kV Ne ion sputtering and annealing in UHV at 800 K. Similar to our previous work on Ir(100),^[49] Co was deposited reactively in an oxygen atmosphere on the sample held at about room temperature using an e-beam evaporator. The Co flux was calibrated by a quartz microbalance and by calibration against previously prepared structures^[50] and adjusted to $\approx 2 \times 10^{13}$ atoms $\text{s}^{-1} \text{cm}^{-2}$. Values given for the coverage Θ refer to a single BL of w-CoO (2.6 Å high), containing 1.1×10^{15} Co ions per cm^2 .

In two of the chambers, oxygen was dosed via a thin, stainless steel tube (“doser”) positioned closely (≤ 20 mm) in front of the sample’s surface, in the third by back-filling the chamber. While the doser enhances the local oxygen pressure by a factor 50 if comparing preparations with the doser close to the surface and 10 cm away. The oxygen partial pressures given in the text remain rough estimates of the local pressures at the sample. As the preparation depends quite sensitively on the combination of Co flux and oxygen partial pressure (see Section 2.1), the final verification of the prepared structure was based on the LEED pattern and its dependence on electron energy.

Computational: The full-dynamical LEED intensity calculations as well as the fitting procedure using the Tensor LEED approximation^[51,52] were carried out using the program package TensErLEED.^[53] The EASiSSS code was used to calculate scattering phase shifts up to angular momenta $\ell = 13$ and the proper energy dependence of the inner potential.^[54] The degree of correspondence of experimental and calculated spectra was quantified by the Pendry R-factor R ,^[55] which also allows to estimate margins of the statistical error via its variance $\text{var}(R)$ (Figure S1, Supporting Information).

For our DFT calculations, we used the Vienna Ab initio Simulation Package (VASP)^[56,57] in the projector-augmented wave (PAW) framework.^[58] The GGA of PBE^[59] for the exchange-correlation functional

was used. The localized nature of the Co d-states was treated by the DFT + U approach of Dudarev with an effective $U_{\text{eff}} = (U - J)$.^[60] For comparison, the HSE^[61] hybrid functional HSE06^[62] was considered as well. The mixing parameter α for the inclusion of exact Hartree–Fock exchange to the PBE functional was varied in the analysis. Following the suggestion of Peng and Perdew,^[42] the PBE + U method was combined with the Tkatchenko–Scheffler (TS)^[63] and Grimme D3 (zero damping)^[64] treatment of van der Waals (vdW) forces. Such an approach is valid on the following grounds: a treatment of transition metal oxides beyond DFT on a many-body level, such as the random-phase approximation, was crucial for the correct description of the polymorphs of ZrO₂,^[65] MnO,^[66] and CoO.^[41] In these theories, both the localized nature of the d-states and vdW interactions are adequately treated, in contrast to the usual DFT functionals. For the latter, these inadequacies could be partially compensated by the inclusion of both Hubbard-like terms^[60] and vdW corrections.^[63,64] Further details are given in the Supporting Information.

Supporting Information

Supporting Information is available from the Wiley Online Library or from the author.

Acknowledgements

This work was supported by the Deutsche Forschungsgemeinschaft (DFG) within the research unit “Functional Molecular Structures on Complex Oxide Surfaces (*funCOS*)” (project no. 214951840), by the Austrian Science Fund (FWF) within SFB F45 (FOXSI), and by computer time from the Vienna Scientific Cluster (VSC).

Open access funding enabled and organized by Projekt DEAL.

Conflict of Interest

The authors declare no conflict of interest.

Data Availability Statement

The data that support the findings of this study are available from the corresponding author upon reasonable request.

Keywords

bandgaps, cobalt oxide, electronic properties, polymorphism, structural analyses

Received: July 14, 2021

Revised: September 9, 2021

Published online: October 1, 2021

- [1] M. Redman, E. Steward, *Nature* **1962**, 193, 867.
- [2] A. S. Risbud, L. P. Snedeker, M. M. Elcombe, A. K. Cheetham, R. Seshadri, *Chem. Mater.* **2005**, 17, 834.
- [3] K. M. Nam, W. S. Seo, H. Song, J. T. Park, *NPG Asia Mater.* **2017**, 9, e364.
- [4] K. Y. Jang, G. Park, K. H. Oh, J. H. Seo, K. M. Nam, *Chem. Commun.* **2017**, 53, 4120.
- [5] A. Ma, H. Park, J. Seo, K. Jang, H. Lee, D. Kim, J. Lee, K. Nam, D.-S. Lee, *Sens. Actuators, B* **2020**, 308, 127698.
- [6] H. Jung, A. Ma, S. A. Abbas, H. Y. Kim, H. R. Choe, S. Y. Jo, K. M. Nam, *Chem. Eng. J.* **2021**, 415, 127958.

- [7] F.-C. Kong, Y.-F. Li, C. Shang, Z.-P. Liu, *J. Phys. Chem. C* **2019**, 123, 17539.
- [8] Y. Wang, H. X. Ge, Y. P. Chen, X. Y. Meng, J. Ghanbaja, D. Horwat, J. F. Pierson, *Chem. Commun.* **2018**, 54, 13949.
- [9] A. Lu, Y. Chen, D. Zeng, M. Li, Q. Xie, X. Zhang, D.-L. Peng, *Nanotechnology* **2013**, 25, 035707.
- [10] J. Fester, M. Garca-Melchor, A. Walton, M. Bajdich, Z. Li, L. Lammich, A. Vojvodic, J. Lauritsen, *Nat. Commun.* **2017**, 8, 14169.
- [11] A. G. Roca, I. V. Golosovsky, E. Winkler, A. López-Ortega, M. Estrader, R. D. Zysler, M. D. Baró, J. Nogués, *Small* **2018**, 14, 1703963.
- [12] I. Golosovsky, M. Estrader, A. López-Ortega, A. Roca, L. López-Conesa, E. D. Corro, S. Estradé, F. Peiró, I. Puente-Orench, J. Nogués, *Appl. Mater. Today* **2019**, 16, 322.
- [13] M. J. Han, J. Yu, *J. Korean Phys. Soc.* **2006**, 48, 1496.
- [14] J. Alaria, N. Cheval, K. Rode, M. Venkatesan, J. M. D. Coey, *J. Phys. D: Appl. Phys.* **2008**, 41, 135004.
- [15] M. J. Han, H.-S. Kim, D. G. Kim, J. Yu, *Phys. Rev. B* **2013**, 87, 184432.
- [16] X. He, W. Zhong, S. Yan, C. Liu, H. Shi, C.-T. Au, Y. Du, *J. Phys. Chem. C* **2014**, 118, 13898.
- [17] Q. Qi, Y. Chen, L. Wang, D. Zeng, D.-L. Peng, *Nanotechnology* **2016**, 27, 455602.
- [18] H. L. Meyerheim, C. Tusche, A. Ernst, S. Ostanin, I. V. Maznichenko, K. Mohseni, N. Jedrecy, J. Zegehnagen, J. Roy, I. Mertig, J. Kirschner, *Phys. Rev. Lett.* **2009**, 102, 156102.
- [19] S. Sindhu, M. Heiler, K.-M. Schindler, W. Widdra, H. Neddermeyer, *Surf. Sci.* **2004**, 566–568, 471.
- [20] W. Meyer, K. Biedermann, M. Gubo, L. Hammer, K. Heinz, *J. Phys.: Condens. Matter* **2008**, 20, 265011.
- [21] K. Biedermann, M. Gubo, L. Hammer, K. Heinz, *J. Phys.: Condens. Matter* **2009**, 21, 185003.
- [22] W. Meyer, K. Biedermann, M. Gubo, L. Hammer, K. Heinz, *Phys. Rev. B* **2009**, 79, 121403.
- [23] L. Gragnaniello, S. Agnoli, G. Parteder, A. Barolo, F. Bondino, F. Allegretti, S. Surnev, G. Granozzi, F. Netzer, *Surf. Sci.* **2010**, 604, 2002.
- [24] I. Sebastian, H. Neddermeyer, *Surf. Sci.* **2000**, 454–456, 771.
- [25] M. A. Arman, L. R. Merte, E. Lundgren, J. Knudsen, *Surf. Sci.* **2017**, 657 90.
- [26] M. De Santis, A. Buchsbaum, P. Varga, M. Schmid, *Phys. Rev. B* **2011**, 84, 125430.
- [27] A. S. Walton, J. Fester, M. Bajdich, M. A. Arman, J. Osiecki, J. Knudsen, A. Vojvodic, J. V. Lauritsen, *ACS Nano* **2015**, 9, 2445.
- [28] J. Fester, A. Walton, Z. Li, J. V. Lauritsen, *J. Phys. Chem. Chem. Phys.* **2017**, 19, 2425.
- [29] J. Fester, Z. Sun, J. Rodríguez-Fernández, A. Walton, J. V. Lauritsen, *J. Phys. Chem. B* **2018**, 122, 561.
- [30] J. Fester, M. Bajdich, A. S. Walton, Z. Sun, P. N. Plessow, A. Vojvodic, J. V. Lauritsen, *Top. Catal.* **2017**, 60, 503.
- [31] I. Sebastian, M. Heiler, K. Meinel, H. Neddermeyer, *Appl. Phys. A: Mater. Sci. Process.* **1998**, 66, S525.
- [32] W. Meyer, D. Hock, K. Biedermann, M. Gubo, S. Müller, L. Hammer, K. Heinz, *Phys. Rev. Lett.* **2008**, 101, 016103.
- [33] R. Freer, *J. Mater. Sci.* **1981**, 16, 3225.
- [34] R. M. Feenstra, *Phys. Rev. B* **1994**, 50, 4561.
- [35] S. Otto, T. Fauster, *J. Phys.: Condens. Matter* **2016**, 28, 055001.
- [36] S. Mandal, K. Haule, K. M. Rabe, D. Vanderbilt, *npj Comput. Mater.* **2019**, 5, 1.
- [37] H. Jiang, R. I. Gomez-Abal, P. Rinke, M. Scheffler, *Phys. Rev. B* **2010**, 82, 045108.
- [38] L. A. Cipriano, G. Di Liberto, S. Tosoni, G. Pacchioni, *J. Chem. Theory Comput.* **2020**, 16, 3786.
- [39] H.-X. Deng, J. Li, S.-S. Li, J.-B. Xia, A. Walsh, S.-H. Wei, *Appl. Phys. Lett.* **2010**, 96, 162508.

- [40] A. Schrön, C. Rödl, F. Bechstedt, *Phys. Rev. B* **2012**, *86*, 115134.
- [41] K. Saritas, J. T. Krogel, F. A. Reboledo, *Phys. Rev. B* **2018**, *98*, 155130.
- [42] H. Peng, J. P. Perdew, *Phys. Rev. B* **2017**, *96*, 100101.
- [43] R. F. W. Bader, *Chem. Rev.* **1991**, *91*, 893.
- [44] M. Yu, D. R. Trinkle, *J. Chem. Phys.* **2011**, *134*, 064111.
- [45] A. Arnaldsen, W. Tang, G. Henkelman, Bader charge analysis V 1.04, <http://theory.cm.utexas.edu/bader/> (accessed: September 2021).
- [46] L. Ivanova, S. Borisova, H. Eisele, M. Dähne, A. Laubsch, P. Ebert, *Appl. Phys. Lett.* **2008**, *93*, 192110.
- [47] V. Portz, M. Schnedler, L. Lymperakis, J. Neugebauer, H. Eisele, J.-F. Carlin, R. Butté, N. Grandjean, R. E. Dunin-Borkowski, P. Ebert, *Appl. Phys. Lett.* **2017**, *110*, 022104.
- [48] R. Schlesinger, F. Bussolotti, J. Yang, S. Sadofev, A. Vollmer, S. Blumstengel, S. Kera, N. Ueno, N. Koch, *Phys. Rev. Mater.* **2019**, *3*, 074601.
- [49] K. Heinz, L. Hammer, *J. Phys.: Condens. Matter* **2013**, *25*, 173001.
- [50] P. Ferstl, L. Hammer, C. Sobel, M. Gubo, K. Heinz, M. A. Schneider, F. Mittendorfer, J. Redinger, *Phys. Rev. Lett.* **2016**, *117*, 046101.
- [51] K. Heinz, *Rep. Prog. Phys.* **1995**, *58*, 637.
- [52] P. J. Rous, J. B. Pendry, D. K. Saldin, K. Heinz, K. Müller, N. Bickel, *Phys. Rev. Lett.* **1986**, *57*, 2951.
- [53] V. Blum, K. Heinz, *Comput. Phys. Commun.* **2001**, *134*, 392.
- [54] J. Rundgren, *Phys. Rev. B* **2003**, *68*, 125405.
- [55] J. B. Pendry, *J. Phys. C: Solid State Phys.* **1980**, *13*, 937.
- [56] G. Kresse, J. Hafner, *Phys. Rev. B* **1993**, *47*, 558.
- [57] G. Kresse, J. Furthmüller, *Comput. Mater. Sci.* **1996**, *6*, 15.
- [58] G. Kresse, D. Joubert, *Phys. Rev. B* **1999**, *59*, 1758.
- [59] J. P. Perdew, K. Burke, M. Ernzerhof, *Phys. Rev. Lett.* **1996**, *77*, 3865.
- [60] S. L. Dudarev, G. A. Botton, S. Y. Savrasov, C. J. Humphreys, A. P. Sutton, *Phys. Rev. B* **1998**, *57*, 1505.
- [61] J. Heyd, G. E. Scuseria, M. Ernzerhof, *J. Chem. Phys.* **2003**, *118*, 8207.
- [62] A. V. Krukau, O. A. Vydrov, A. F. Izmaylov, G. E. Scuseria, *J. Chem. Phys.* **2006**, *125*, 224106.
- [63] A. Tkatchenko, M. Scheffler, *Phys. Rev. Lett.* **2009**, *102*, 073005.
- [64] S. Grimme, J. Antony, S. Ehrlich, H. Krieg, *J. Chem. Phys.* **2010**, *132*, 154104.
- [65] W. Mayr-Schmölzer, J. Planer, J. Redinger, A. Grüneis, F. Mittendorfer, *Phys. Rev. Res.* **2020**, *2*, 043361.
- [66] H. Peng, S. Lany, *Phys. Rev. B* **2013**, *87*, 174113.
- [67] G. von Witte, T. Kißlinger, J. G. Horstmann, K. Rossnagel, M. A. Schneider, C. Ropers, L. Hammer, *Phys. Rev. B* **2019**, *100*, 155407.
- [68] A. Schrön, C. Rödl, F. Bechstedt, *Phys. Rev. B* **2010**, *82*, 165109.
- [69] I. Battisti, V. Fedoseev, K. M. Bastiaans, A. de la Torre, R. S. Perry, F. Baumberger, M. P. Allan, *Phys. Rev. B* **2017**, *95*, 235141.
- [70] F. Pedregosa, G. Varoquaux, A. Gramfort, V. Michel, B. Thirion, O. Grisel, M. Blondel, P. Prettenhofer, R. Weiss, V. Dubourg, J. Vanderplas, A. Passos, D. Cournapeau, M. Brucher, M. Perrot, E. Duchesnay, *J. Mach. Learn. Res.* **2011**, *12*, 2825.